INL/JOU-23-72180-Revision-0

Frequency Resilience Enhancement for Power Systems with High Penetration of Grid-Forming Inverters

March 2023

Jianzhong Gui, Hangtian Lei, Timothy R. McJunkin, Brian K. Johnson

Changing the World's Energy Future

INL/JOU-23-72180-Revision-0

Frequency Resilience Enhancement for Power Systems with High Penetration of Grid-Forming Inverters

Jianzhong Gui, Hangtian Lei, Timothy R. McJunkin, Brian K. Johnson

March 2023

Idaho National Laboratory
Idaho Falls, Idaho 83415

http://www.inl.gov

Prepared for the
U.S. Department of Energy
Under DOE Idaho Operations Office
Contract DE-AC07-05ID14517

Frequency Resilience Enhancement for Power Systems with High Penetration of Grid-Forming Inverters

Jianzhong Gui, Hangtian Lei, Timothy R. McJunkin, and Brian K. Johnson

***Abstract*—Grid following inverter-based renewable generation has replaced conventional generation in recent years, resulting in lower system inertia. The frequency resilience in such a lower inertia system is critical for emergency mitigation. In this paper, we propose a resilience metric based on frequency recovery to quantitatively represent system resilience in terms of the rate of change of frequency. Application of grid-forming converters provides a means to improve system resilience by providing virtual inertia. An under-frequency load shedding strategy is applied to further support frequency recovery in cases with high penetration of grid-forming inverters. Case studies are designed and performed in a modified IEEE 9-bus test system using the PSCAD/EMTDC platform. Simulation results demonstrate the validity of the proposed resilience metric and the effectiveness of the strategy for reducing frequency excursion in inverter-based power systems.**

***Index Terms*—Frequency, grid-forming inverter, resilience, renewable generation, under-frequency load shedding.**

I. Introduction

Modern power systems are undergoing a transition to include more renewable wind and photovoltaic (PV) energy resources which couple to the power grid through inverters [1]. Most of these inverters are controlled to rapidly track grid frequency and phase angle in order to maintain peak power transfer for the resource. The increasing penetration of grid-following inverter-based resources (IBRs) leads to a lower inertia for system control and operation, and brings frequency stability concerns [2]-[5]. The frequency resilience evaluation and enhancement are critically important under the trend of increasing renewable energy generation, and thus need to be investigated for power systems with inverter-based generation.

Historically, system frequency has been supported by synchronous machines (SMs). Theoretically, the inverters used in IBRs have the ability to vary output power promptly to match demand to maintain system frequency [2]. However, doing so requires either operating the wind and PV resources below their maximum power points with associated lost revenue or adding significant amounts of energy storage. The system frequency is still maintained by SMs at present with minor support from energy storage systems [3]. A system with very high percentages of inverter-based renewable resources requires alternative approaches to support frequency. Frequency resilience enhancement mainly includes two major aspects. One is to design better controllers for inverters, and the other is to cooperate with other operation techniques.

To improve frequency resilience, researchers are developing new designs of inverter controllers. Grid-following (GFL) inverters acting as a fast-responding current sources and grid-forming (GFM) inverters acting as a voltage source are the main inverter categories applied into power systems literature [4], [5]. Grid-forming inverters can be controlled to share several same characteristics with SMs [6]-[10]. Additionally, GFM inverters have the ability of changing power output to balance load and contributing to the regulation of frequency [8]-[14] when connected to a resource that has the ability to regulate output power on command, such as an energy storage system or a PV system that is operated below its maximum power point. Reference [9] designed a droop-controlled grid-forming controller to support frequency under both over and under frequency events. It also verifies that the droop-controlled GFM inverters achieve a better frequency response than the frequency-watt GFL inverters. The authors of [10] performed a frequency response comparison between GFL and GFM converters. To set frequency directly, the authors of [11] proposed a grid-forming frequency shaping control strategy using a first-order coherent dynamics function. The frequency reached an equilibrium level without dropping to a deep frequency nadir. The authors in [12] and [13] came up with the duality characteristics of GFL and GFM inverters to strengthen dynamic frequency stability for inverter-based networks, providing a new option to control inverter-based generation. Similarly, frequency characteristics based on various GFM control techniques are compared with conventional SMs in [14] and [15], and effective frequency response was highlighted for GFM inverters when interacting with SMs during under-frequency events. A new droop control based on *angle-frequency* was proposed as an alternative to a *power-frequency* scheme in [16], where the inverter continues to support system frequency under the current limitation of GFM inverters.

Under-frequency load shedding (UFLS) schemes are widely used to frequency regulation in the face of major disturbances [17]-[24], and will become increasingly necessary in heavily loaded systems with very high penetration of GFM and GFL IBRs. An UFLS scheme was applied in inverter-base microgrid in [17]-[20] with distributed energy resources whose inverters are working in grid-forming mode. But the capacity of these IBRs is limited to provide frequency support in a higher voltage level system, and the frequency response is discussed in islanded conditions. Therefore, the authors in [21] and [22] proposed

This work was supported through the INL Laboratory Directed Research and Development (LDRD) Program under DOE Idaho Operations Office Contract DE-AC07-05ID14517.

J. Gui, H. Lei, and B. K. Johnson are with the Department of Electrical and Computer Engineering, University of Idaho, Moscow, ID 83843, USA (emails: gui2361@vandals.uidaho.edu; hlei7@uidaho.edu; bjohnson@uidaho.edu).

T. R. McJunkin is with Idaho National Laboratory, Idaho Falls, ID 83415, USA (email: timothy.mcjunkin@inl.gov).

multi-stage UFLS schemes to restore power balance against frequency instability. Although the islanded operation was taken into consideration, the dynamic characteristic of IBRs was neglected, especially how the IBRs response to severe frequency events. Similarly, traditional UFLS schemes in [23] and [24] were upgraded to improve system frequency resilience. However, the simulated distributed generators were wind turbines modeled with unchanged power outputs during the period of the event, which brings no contribution to support system frequency response. In summary, the much research focuses on UFLS for power system with IBRs aim to improve UFLS schemes, but have not coordinated these schemes with the frequency support ability from GFM IBRs.

The contributions of this paper include studying frequency response ability of GFM inverters, constructing an evaluation metric for frequency response, and cooperating with UFLS schemes to enhance frequency resilience. The remainder of this paper is organized as follows. Section II presents the modeling of multi-loop droop GFM inverters. The frequency resilience metric with mitigation strategy based on UFLS schemes is proposed and demonstrated in Section III. The designed case studies are performed on a modified IEEE 9-bus system in Section IV. Finally, conclusions and future work are discussed in Section V.

II. Modelling of Grid-Forming Inverters

The categories of existing grid-forming controllers mainly include droop controllers, virtual synchronous machines, and virtual oscillators [1]. Each type of controller acts as a voltage source with an amplitude and frequency, which are affected by reactive generation and system load, respectively. The most widely used grid-forming method, droop control, exhibits a linear trade-off between frequency and voltage, which is similar to a steady-state synchronous machine. The control scheme and controller equations of droop control GFM inverter proposed in [3]-[5], [25], [26] are summarized in this section and used in this paper. The diagram of droop control is shown in Fig. 1.

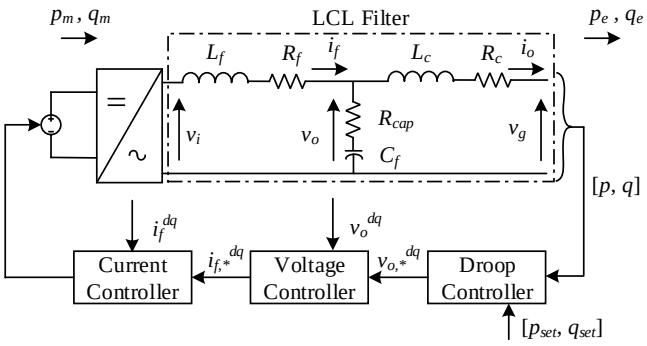

Fig. 1. Control system diagram of grid-forming voltage source converter

The voltage and current controllers are separately regulated with a proportional integral controller, which processes the variables in a rotating direct-quadrature (*dq*) reference frame. Within the control schemes, all the three-phase voltages and currents are transformed according to (1):

$$\begin{bmatrix} v_d \\ v_q \end{bmatrix} = T_{dq} \cdot \begin{bmatrix} v_a \\ v_b \\ v_c \end{bmatrix}, \begin{bmatrix} i_d \\ i_q \end{bmatrix} = T_{dq} \cdot \begin{bmatrix} i_a \\ i_b \\ i_c \end{bmatrix} \tag{1}$$

where T_{dq} is the Park's transformation matrix shown in (2). It transforms 3-phase *abc* variables to 2-axis *dq* variables.

$$T_{dq} = \frac{2}{3}\begin{bmatrix} \cos(\theta) & \cos(\theta - \frac{2\pi}{3}) & \cos(\theta + \frac{2\pi}{3}) \\ \sin(\theta) & \sin(\theta - \frac{2\pi}{3}) & \sin(\theta + \frac{2\pi}{3}) \end{bmatrix} \tag{2}$$

where θ is the rotating reference angle for controller calculation, which is acquired from the droop controller characteristics shown in (3):

$$\begin{aligned} \dot{\theta} &= \omega_n + M_p(p^{set} - p_m) \\ v_{o,*}^q &= v_{o,set}^q + M_q(q^{set} - q_m) \end{aligned} \tag{3}$$

where ω_n is the base system frequency, which equals to 60 Hz. M_p and M_q are the frequency and voltage droop gains. p^{set} and q^{set} are the real and reactive power set points of electrical power outputs of inverter. In *dq* domain, $v_{o,*}^q$ is the voltage set point of filter capacitor, C_f, and $v^q{}_{o,set}$ is the rated voltage set-point of the filter capacitor. p_m and q_m represent the initial real and reactive power converted by GFM inverters. They are defined in (4) and generate from the values of instantaneous real and reactive power (p_e and q_e) passing through a low-pass filter in this paper, whose cutoff frequency is ω_{fil}.

$$\begin{aligned} \dot{p_m} &= \omega_{fil}(p_e - p_m) \\ \dot{q_m} &= \omega_{fil}(q_e - q_m) \end{aligned} \tag{4}$$

where p_e and q_e are calculated using the *dq* components from the measured voltage and current at the point of interconnect using equation (1).

The current through the filter resistor R_f, inductor L_f, and the voltage across the filter capacitor C_f are regulated by the current controllers and voltage controllers. Pertinent equations are shown in (5) and (6):

$$\begin{aligned} \dot{\xi}^{dq} &= v_o^{dq} - v_{o,*}^{dq} \\ i_{f,*}^{dq} &= K_V^i \xi^{dq} + K_V^p \dot{\xi}^{dq} - j\omega C_f v_o^{dq} + G_V i_o^{dq} \end{aligned} \tag{5}$$

$$\begin{aligned} \dot{\gamma}^{dq} &= i_f^{dq} - i_{f,*}^{dq} \\ v_{i,*}^{dq} &= K_C^i \gamma^{dq} + K_C^p \dot{\gamma}^{dq} - j\omega L_f i_f^{dq} + G_C v_o^{dq} \end{aligned} \tag{6}$$

where ξ^{dq} and γ^{dq} are the integrator error states; $K_V{}^i$ and $K_C{}^i$ are the integral gains; $K_V{}^p$ and $K_C{}^p$ are the proportional gains. G_V and G_C are the voltage and current feed forward gains, respectively. ω is the radian frequency from the droop relation.

III. Frequency Resilience Mitigation Based on Under Frequency Load Shedding

Typically, system frequency response to disturbances involves two stages: frequency decaying (or rising) and frequency recovery stages, when system is affected by loss of generation (or large load increase). Usually, the action of UFLS is performed to avoid reaching an unacceptable frequency level. Reaching a worse frequency level will probably result in tripping additional generation and even blackout in several areas. This issue becomes much more critical in power systems with high proportions of IBRs generation because of the low system inertia. To quantify the system resilience in terms of frequency, we propose the metric based on frequency change curve, with details illustrated in this section.

A. *The Proposed Frequency Resilience Metric*

The frequency curve in Fig. 2 shows that the event occurring at t_1 in system causes system frequency reaching the nadir point of f_n Hz at t_2, and the frequency recovered to a stable level of f_t Hz at t_3. The entire process includes frequency decaying and frequency recovery. In contrast, the system has a similar frequency recovery process during the over-frequency event, but f_n would be a peak value of the frequency at t_2. In this way, one metric proposed to consider the pre-event and post-event periods is an effective indicator to evaluate system frequency resilience.

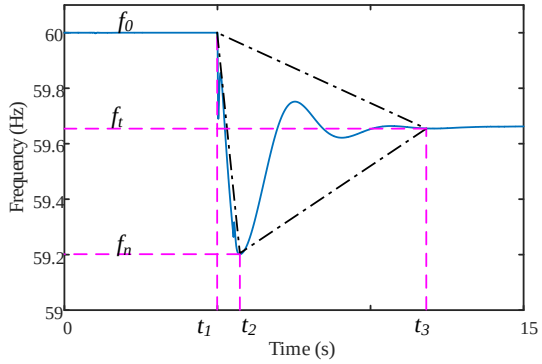

Fig. 2. Frequency curve schematic during an underfrequency event.

The area of frequency recovery, which is the proposed resilience metric, is shown in (7):

$$R_f = \left|\frac{f_t - f_n}{t_r}\right| + \left|\frac{f_0 - f_n}{t_{d/r}}\right| \tag{7}$$

where t_r is the frequency recovery time that equals to t_3-t_2, and $t_{d/r}$ is the frequency decaying or rising time that equals to t_2-t_1. f_0 is the nominal frequency of the system.

The first part in (7) is modeled as a slope during the frequency rising process, as shown in the dash-dotted line between t_2 and t_3 in Fig. 2. The slope valued the second part in (7) is smaller than the fastest rate of change of frequency (ROCOF) when the event occurs. The fastest ROCOF is the first derivative of the fundamental frequency at t=0 [27], [28]. The ROCOF is defined in (8):

$$\frac{df}{dt} = \frac{-30 \cdot \Delta L}{H} \cdot e^{\frac{D \cdot t}{2 \cdot H}} \tag{8}$$

where ΔL is the value of load change, H is the system inertia, D is the value of load-damping.

The proposed resilience metric considers frequency change in frequency decaying (or rising) and frequency recovery stages. The two slopes represent how fast the frequency is decaying (rising) and recovering. For a system, a bigger metric value means that the corresponding frequency regulation scheme is more effective when compared under the same disturbance, which indicates that the system has a better ability to achieve frequency recovery. Methods for determining specific thresholds of the proposed metric will be part of our future work.

B. *UFLS-Based Frequency Resilience Mitigation Strategy*

The frequency is related to the balance between generation and load including system power loss. When a loss of generation or load occurs, the system frequency decays or rises in a short period, and then transits to a new level. The new frequency could be the nominal system frequency, another acceptable levels, or the severe levels. For a power system with inverter-based resources, the under-frequency event could still cause damages to the existing steam turbines and hydroelectric turbines. Therefore, the under-frequency load shedding should be used in such power systems. The basic diagram of UFLS is shown in Fig. 3, which will be applied in the following emulations.

The inputs of the UFLS controller are the measured system frequency (f_m), the rate of change of frequency (df/dt), and enabled generator tripping signals (BRK_G) at time t. The outputs are the amounts of shedded load according to their priorities.

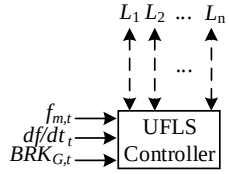

Fig. 3. UFLS control logics.

The UFLS controller includes three different under-frequency levels as shown in Table I. The frequency thresholds are set as 59.3 Hz, 59.0 Hz, and 58.7 Hz for each level. The proportion of accumulated load relief is between 30% and 45% of the peak load.

TABLE I. UFLS LEVELS AND SHEDDING PROPORTION OF LOAD

UFLS Level	Frequency Threshold (Hz)	Minimum Proportion (%)	Maximum Proportion (%)
1	59.3	10	25
2	59.0	10	10
3	58.7	10	10

The maximum total shedded load at each level is arranged referring to the amount of load that is able to relief. The amount of load relief is calculated by (9):

$$L_{shed} = \alpha \cdot 2H \cdot \frac{S_{Base}}{f_0} \cdot \frac{df}{dt} \tag{9}$$

where α is the inertia correction factor of load between 1.0 and 1.5, to correct the amount of load relief. S_{Base} is system generator MVA base.

IV. CASE STUDY

A. *Testing System Description*

A modified IEEE 9-bus system is used as the test system in this section. The one-line diagram of the test system is shown in Fig. 4, and the penetration of GFM converters is shown in Table II. The synchronous machines with exciter and governor are replaced by GFM converters depending on the penetration percentages in the following simulations.

TABLE II. GFM CONVERTER PENETRATION

Case No.	Synchronous Generation (MW)	Converter Generation (MW)	Replaced Generator	Penetration (%)
1	319.63	0	-	0
2	156.63	163.00	G2	51.00
3	85	234.63	G1, G2	73.41
4	0	319.63	G1, G2, G3	100

Simulations are performed using PSCAD/EMTDC. The network parameters are referred from the PSCAD technical notes of IEEE 9-bus system. The model of the grid-forming voltage source converter implemented in this paper is based on the principles and parameters described in [25] and [26]. The simulation time is set as 20 s, and events are set to occur at t=7 s in different scenarios. All loads in this test system are selected as sheddable loads, and the UFLS schemes are set to be triggered when system frequency is below the threshold in each level.

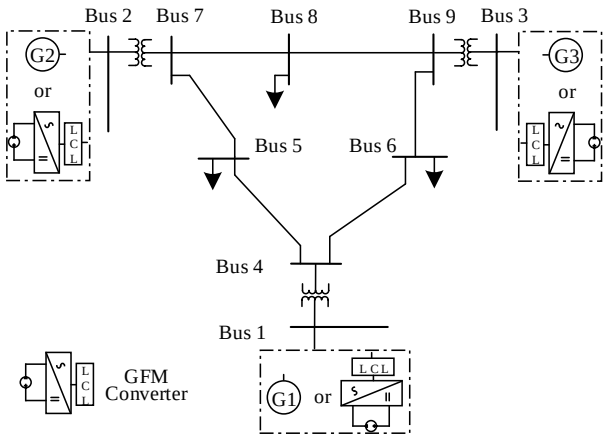

Fig. 4. One-line diagram of the modified IEEE 9-bus test system.

B. Frequency Response With Penetration of GFM Converter

The frequency response is tested under the condition of under-frequency events. The sudden deficiency of power leads the system to an under-frequency status which needs to be handled by adjusting other generation sources or other active actions to prevent frequency decaying. With the increasing penetration of GFM inverters, the frequency curves are compared with the one with 100% synchronous machines.

1) Frequency Response of Rising Loads

The under-frequency event is to increase the load at Bus 8. The 10% increased amount of loads results in insufficiency of power, so that the system frequency experiences an under-frequency period, as shown in Fig. 5 with the frequency resilience values.

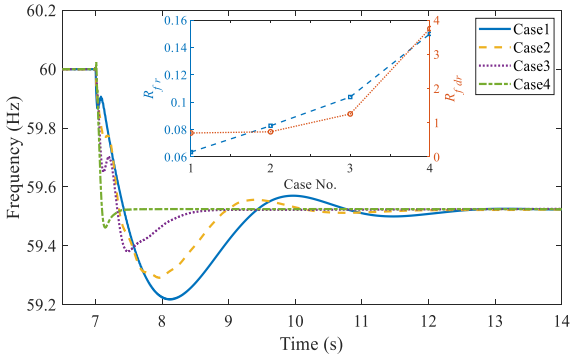

Fig. 5. Frequency curves and resilience values of for rising loads.

From Fig. 5, it can be seen that with the increasing penetration of GFM, the frequency reaches a higher nadir in a shorter time, and the rate of recovery is increased, even with a higher decaying rate. The proposed metric values also show that frequency is faster affected with higher penetration of GFM, and the transient period is shortened due to reduced system inertia.

2) Frequency Response of Tripping Generations

The under-frequency event is caused by tripping the generation device at Bus 3. The frequency curves and the values of frequency resilience metric are shown in Fig. 6.

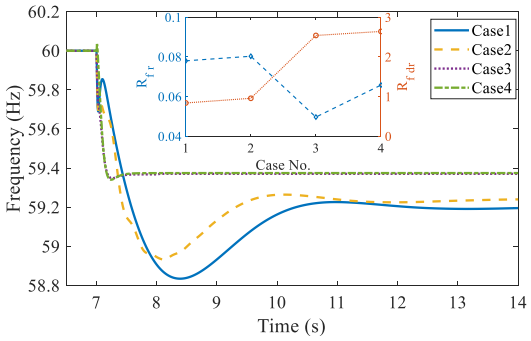

Fig. 6. Frequency curves and resilience values for tripping generations.

From Fig. 6, we can observe that the frequency nadir is lower than the one with relatively lower GFM penetration. The rate of recovery cannot keep the similar trend as shown in Fig. 5, but the rate of decay keeps increasing. It shows that the sensitivity of tripped generation is not linear with GFM penetrations, and higher penetration cannot linearly provide a faster frequency recovery rate. Therefore, remedial actions are needed to regulate system frequency in such scenarios.

C. UFLS-Based Frequency Mitigation

As shown in Fig. 5 and Fig. 6, the frequency nadir is lower than the thresholds in Table I. The enabled UFLS schemes will be triggered in this test system. The time delay of UFLS is 6 cycles for L1 and 30 cycles for L2 and L3. The frequency curves are shown in Fig. 7, and the proposed metric values compared to those values in Fig. 6 are shown in Fig. 8.

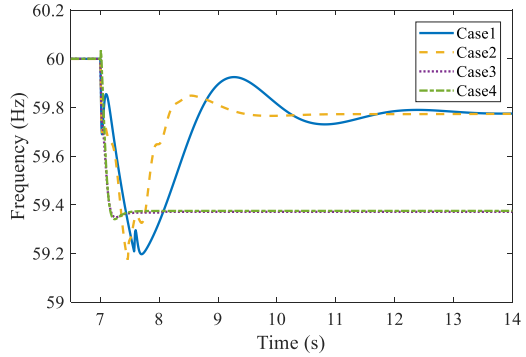

Fig. 7. Frequency curves for tripping generations with UFLS.

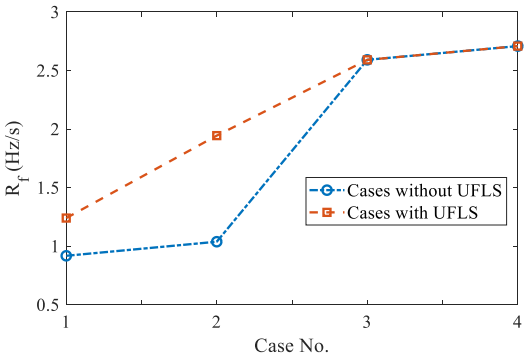

Fig. 8. Frequency resilience values for tripping generations with UFLS.

From Fig. 7 and Fig. 8, it can be seen that Case 3 and Case 4 did not trigger UFLS schemes. The frequency nadirs in Case 1 and Case 2 were brought forward when compared to the time instants in Fig. 6. That means the frequency damping of the system is increased with a higher penetration of GFM inverters, and the UFLS schemes contribute to frequency recovery with penetration of GFM inverters. The higher metric value shows the better resilience of frequency regulation during under-frequency events.

V. CONCLUSION

In this paper, grid-forming inverters are applied to evaluate the impact of penetration inverter-based resources. A resilience metric is proposed based on the recovery process of system frequency, considering the frequency decaying and rising periods to calculate metric values. The validity of the proposed resilience metric is verified with simulations in the modified IEEE 9-bus system. The proposed resilience metric clearly shows the impact of the events on system status and the ability of frequency recovery. The benefit of applying under-frequency load shedding is analyzed in high penetration of inverter-based power systems, which highlights a feasible frequency regulation method.

The applicability of the proposed resilience metric to dynamic frequency regulation processes will be investigated in our future work. Also, the improved inverter controllers with UFLS schemes will be designed to enhance the frequency stability of GFM penetrated power systems.

REFERENCES

[1] Y. Lin, J.H. Eto, B.B. Johnson, J.D. Flicker, R.H. Lasseter, H.N. Villegas Pico, G.S. Seo, B.J. Pierre and A. Ellis, "*Research roadmap on grid-forming inverters*," No. NREL/TP-5D00-73476. National Renewable Energy Lab.(NREL), Golden, CO (United States), 2020.

[2] R. H. Lasseter, Z. Chen and D. Pattabiraman, "Grid-Forming Inverters: A Critical Asset for the Power Grid," IEEE Journal of Emerging and Selected Topics in Power Electronics, vol. 8, no. 2, pp. 925-935, June 2020.

[3] D. Pattabiraman, R. H. Lasseter. and T. M. Jahns, "Comparison of Grid Following and Grid Forming Control for a High Inverter Penetration Power System," *2018 IEEE Power & Energy Society General Meeting (PESGM)*, pp. 1-5, 2018.

[4] D.B. Rathnayake, M. Akrami, C. Phurailatpam, S.P. Me, S. Hadavi, G. Jayasinghe, S. Zabihi and B. Bahrani, "Grid Forming Inverter Modeling, Control, and Applications," *IEEE Access*, vol. 9, pp. 114781-114807, 2021.

[5] W. Du, F.K. Tuffner, K.P. Schneider, R.H. Lasseter, J. Xie, Z. Chen and B. Bhattarai, "Modeling of Grid-Forming and Grid-Following Inverters for Dynamic Simulation of Large-Scale Distribution Systems," *IEEE Transactions on Power Delivery*, vol. 36, no. 4, pp. 2035-2045, Aug. 2021.

[6] T. Zhang, "Impacts of Inverter Control Strategies on the Stability of Low-Inertia Power Systems," *2020 IEEE Power & Energy Society General Meeting (PESGM)*, pp. 1-5, 2020.

[7] M. M. Islam, K. M. Muttaqi, D. Sutanto, M. M. Rahman and O. Alonso, "Controller Design for Grid Forming Inverter-Based Power Generating Systems to Behave as Synchronous Machines," *2021 IEEE Industry Applications Society Annual Meeting (IAS)*, pp. 1-7, 2021.

[8] Z. Zhou, W. Wang, T. Lan and G. M. Huang, "Dynamic Performance Evaluation of Grid-Following and Grid-Forming Inverters for Frequency Support in Low Inertia Transmission Grids," *2021 IEEE PES Innovative Smart Grid Technologies Europe (ISGT Europe)*, pp. 01-05, 2021.

[9] M. E. Elkhatib, W. Du and R. H. Lasseter, "Evaluation of inverter-based grid frequency support using frequency-watt and grid-forming PV inverters", *2018 IEEE Power & Energy Society General Meeting (PESGM)*, pp. 1-5, Aug. 5–10, 2018.

[10] D. A. Kez, A. M. Foley and D. J. Morrow, "Analysis of Fast Frequency Response Allocations in Power Systems With High System Non-Synchronous Penetrations," *IEEE Transactions on Industry Applications*, vol. 58, no. 3, pp. 3087-3101, May-June 2022.

[11] Y. Jiang, A. Bernstein, P. Vorobev and E. Mallada, "Grid-Forming Frequency Shaping Control for Low-Inertia Power Systems," *IEEE Control Systems Letters*, vol. 5, no. 6, pp. 1988-1993, Dec. 2021.

[12] Y. Gu and T. C. Green, "Power System Stability With a High Penetration of Inverter-Based Resources," *Proceedings of the IEEE*, 2022.

[13] Y. Li, Y. Gu and T. Green, "Revisiting Grid-Forming and Grid-Following Inverters: A Duality Theory," *IEEE Transactions on Power Systems*, 2022.

[14] F. Gonzalez-Longatt, J. L. Rueda, P. Palensky, H. R. Chamorro and V. Sood, "Frequency Support provided by Inverted Based-Generation using Grid-Forming Controllers: A Comparison during Islanded Operation," *2021 IEEE Electrical Power and Energy Conference (EPEC)*, pp. 113-118, 2021.

[15] A. Tayyebi, D. Groß, A. Anta, F. Kupzog and F. Dörfler, "Frequency Stability of Synchronous Machines and Grid-Forming Power Converters," *IEEE Journal of Emerging and Selected Topics in Power Electronics*, vol. 8, no. 2, pp. 1004-1018, June 2020.

[16] J. Erdocia, A. Urtasun and L. Marroyo, "Power Angle–Frequency Droop Control to Enhance Transient Stability of Grid–Forming Inverters under Voltage Dips," *IEEE Journal of Emerging and Selected Topics in Power Electronics*, 2022.

[17] S. Rahmani, A. Rezaei-Zare, M. Rezaei-Zare and A. Hooshyar, "Voltage and Frequency Recovery in an Islanded Inverter-Based Microgrid Considering Load Type and Power Factor," *IEEE Transactions on Smart Grid*, vol. 10, no. 6, pp. 6237-6247, Nov. 2019.

[18] J. Choi, A. Khalsa, D. A. Klapp, S. Baktiono and M. S. Illindala, "Survivability of Prime-Mover Powered Inverter-Based Distributed Energy Resources During Microgrid Islanding," *IEEE Transactions on Industry Applications*, vol. 55, no. 2, pp. 1214-1224, March-April 2019.

[19] A. Kannan, M. Nuschke, B.P. Dobrin and D. Strauß-Mincu, "Frequency stability analysis for inverter dominated grids during system split." *Electric Power Systems Research* vol. 188, pp. 106550, 2020.

[20] E. Dehghanpour, H. K. Karegar and R. Kheirollahi, "Under Frequency Load Shedding in Inverter Based Microgrids by Using Droop Characteristic," *IEEE Transactions on Power Delivery*, vol. 36, no. 2, pp. 1097-1106, April 2021.

[21] A. A. koosha and T. Amraee, "Under Frequency Load Shedding Against Severe Generation Outages in Low Inertia Power Grids," *2020 15th International Conference on Protection and Automation of Power Systems (IPAPS)*, pp. 108-114, 2020.

[22] A. Darbandsari, T. Amraee, "Under frequency load shedding for low inertia grids utilizing smart loads." *International Journal of Electrical Power & Energy Systems*, vol. 135, pp. 107506, 2022.

[23] M. N. H. Shazon, S. R. Deeba and S. R. Modak, "A Frequency and Voltage Stability-Based Load Shedding Technique for Low Inertia Power Systems," *IEEE Access*, vol. 9, pp. 78947-78961, 2021.

[24] S. Gordon, C. Mcgarry, K. Bell and J. Tait, "Impact of Low Inertia and High Distributed Generation on the Effectiveness of Under Frequency Load Shedding Schemes," *IEEE Transactions on Power Delivery*, 2021.

[25] R. W. Kenyon, A. Sajadi, A. Hoke and B.-M. Hodge, "Open-Source PSCAD Grid-Following and Grid-Forming Inverters and a Benchmark for Zero-Inertia Power System Simulations", *2021 IEEE Kansas Power and Energy Conference*, 2021.

[26] A. Sajadi, R. W. Kenyon, M. Bossart and B. M. Hodge, "Dynamic Interaction of Grid-Forming and Grid-Following Inverters with Synchronous Generators in Hybrid Power Plants," *2021 IEEE Kansas Power and Energy Conference (KPEC)*, pp. 1-6, 2021.

[27] P. Kundur, "Load Response to Frequency Deviation," *Power System Stability and Control*, McGraw-Hill, Inc., 1994, pp. 584–587.

[28] P. Kundur, "Factors Influencing Frequency Decay," *Power System Stability and Control*, McGraw-Hill, Inc., 1994, pp. 625.